NANO LETTERS

pubs.acs.org/NanoLett

Letter

Dissecting Interlayer Hole and Electron Transfer in Transition Metal Dichalcogenide Heterostructures via Two-Dimensional Electronic Spectroscopy

Veronica R. Policht, Mattia Russo, Fang Liu, Chiara Trovatello, Margherita Maiuri, Yusong Bai, Xiaoyang Zhu,* Stefano Dal Conte,* and Giulio Cerullo*

Cite This: *Nano Lett.* 2021, 21, 4738−4743

Read Online

ACCESS | Metrics & More | Article Recommendations | Supporting Information

ABSTRACT: Monolayer transition metal dichalcogenides (ML-TMDs) are two-dimensional semiconductors that stack to form heterostructures (HSs) with tailored electronic and optical properties. TMD/TMD-HSs like WS_2/MoS_2 have type II band alignment and form long-lived (nanosecond) interlayer excitons following sub-100 fs interlayer charge transfer (ICT) from the photoexcited intralayer exciton. While many studies have demonstrated the ultrafast nature of ICT processes, we still lack a clear physical understanding of ICT due to the trade-off between temporal and frequency resolution in conventional transient absorption spectroscopy. Here, we perform two-dimensional electronic spectroscopy (2DES), a method with both high frequency and temporal resolution, on a large-area WS_2/MoS_2 HS where we unambiguously time resolve both interlayer hole and electron transfer with 34 ± 14 and 69 ± 9 fs time constants, respectively. We simultaneously resolve additional optoelectronic processes including band gap renormalization and intralayer exciton coupling. This study demonstrates the advantages of 2DES in comprehensively resolving ultrafast processes in TMD-HS, including ICT.

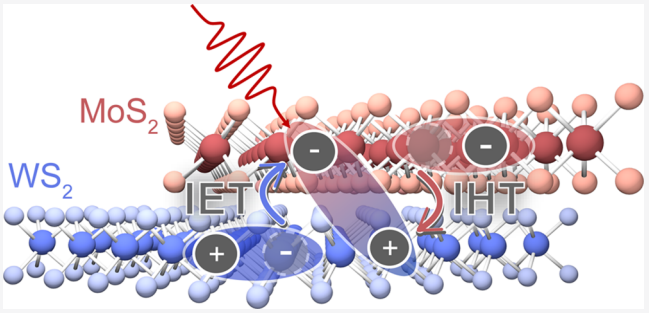

KEYWORDS: *transition metal dichalcogenides, van der Waals heterostructure, interlayer charge transfer, ultrafast spectroscopy*

Semiconducting monolayer transition metal dichalcogenides (ML-TMDs) are a class of two-dimensional crystalline materials with enticing electronic and optical properties,[1,2] including a direct band gap in the visible range, strong light−matter coupling, enhanced excitonic correlations, and spin/valley locking.[3−5] A growing area of TMD research involves vertical stacks of ML-TMDs, referred to as TMD heterostructures (HSs).[6,7] Weak interlayer van der Waals forces between ML-TMDs bypass the lattice parameter matching constraints of conventional semiconductor HSs and preserve the electronic structure of each constituent, enabling the creation of new materials with tailored electronic and optical properties which differ from those of the isolated MLs.

Several TMD-HSs present a type II (staggered) band alignment, in which the valence band (VB) maximum and the conduction band (CB) minimum at the K/K′ points reside in different layers. This alignment favors charge separation and the formation of interlayer (IL) excitons via interlayer charge transfer (ICT). IL excitons are of particular interest as they feature recombination time scales (i.e., 1−100 ns)[8−10] orders of magnitude longer than those of intralayer excitons in isolated ML-TMDs (i.e., ∼100 ps).[11] The strong enhancement of the IL exciton lifetime, due to a reduced spatial overlap of the electron and hole wave functions, is responsible for the observation of several phenomena including the diffusion of IL excitons over micrometer length scales[12,13] and extremely long valley polarization retention,[14,15] among others. Enhanced IL exciton lifetimes make TMD-HSs with type II band alignment excellent candidates for optoelectronic and light-harvesting applications.[16]

A variety of spectroscopic techniques, including photoluminescence and ultrafast transient absorption (TA) spectroscopy, have revealed ICT in TMD-HSs[17,18] to be extremely rapid[19−26] and very efficient.[23] ICT has been previously reported to occur on a sub-100 fs time scale,[19−26] though there remains uncertainty in the rates of ICT and a lack of information about differences in electron versus hole transfer times within the same system. Several studies on IL electron transfer have used above-resonance excitation, which introduces additional many-body effects into the system, and it is

Received: March 18, 2021
Revised: May 12, 2021
Published: May 26, 2021

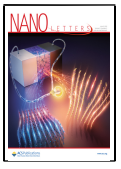

https://doi.org/10.1021/acs.nanolett.1c01098
Nano Lett. 2021, 21, 4738−4743

unclear how to disentangle these effects from ICT processes. Experimental studies show that the time scales and efficiencies of ICT are independent of the IL twist angle.[21,24,25,27] Several theories as to how ICT proceeds without hindrance by interlayer momentum mismatch include mediation via local structural inhomogeneity,[25] excess electronic energy,[21,23] phonon-mediated intermediate scattering through hybridized valleys,[26,28−32] and long-lived quantum coherences at the interface.[33]

Obtaining a comprehensive picture of ICT processes in TMD-HSs is of critical importance both for understanding the fundamental physics at play and for developing optoelectronic applications. One key experimental limitation in ultrafast TA studies of ICT thus far has been the trade-off between temporal and spectral resolution. Ultrafast TA spectroscopy is limited in its ability to distinguish between transitions in spectrally congested systems, where electronic transitions are close in energy. In fact, spectral selection of one transition requires narrowband pump pulses which, due to the Fourier transform (FT) limitation, reduce the temporal resolution of the experiment.

Two-dimensional electronic spectroscopy (2DES) is a multidimensional spectroscopy technique that measures the third-order material polarization using a sequence of three pulses: two excitation pulses separated by the so-called coherence time, t_1, and a detection pulse that is delayed by the waiting time, t_2, with respect to the second excitation pulse (Figure 1a). FT over the coherence time t_1 allows for

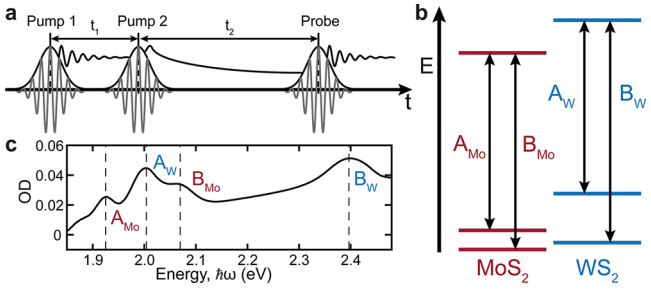

Figure 1. (a) 2DES pulse scheme. Two pump pulses are separated by the coherence time, t_1, and are followed by a probe pulse delayed by the waiting time, t_2. Scanning and Fourier transforming t_1 yields the excitation frequency axis (ω_1). (b) Electronic energy levels of the A and B excitons of the WS_2/MoS_2 HS. (c) 80 K linear absorption spectrum of the WS_2/MoS_2 HS with labeled peaks for the A and B excitons.

resolution over the excitation frequency axis, while resolution over the detection frequency axis is typically obtained by dispersing the detection pulse in a spectrometer.[34−36] 2DES can obtain high excitation frequency resolution while using broadband pulses and thus simultaneously maximize spectral and temporal resolution. 2DES is very well-suited for studying ultrafast dynamics in systems with a high degree of spectral congestion[37] and has been exploited to measure inhomogeneous/homogeneous line widths,[38−41] excitonic coupling,[42−44] exciton valley coherence,[39] and biexcitons[38] in ML-TMDs.

Here, we use 2DES to simultaneously measure both interlayer electron and hole transfer dynamics in a large-area WS_2/MoS_2 HS prepared using a novel mechanical exfoliation technique.[45] This is achieved by using extremely short (sub-20 fs) and broadband pulses with spectra covering the A and B exciton of MoS_2 and the A exciton of WS_2. We observe signatures of intra- and interlayer coupling between the A/B excitons of MoS_2 and the A exciton of WS_2 immediately after photoexcitation. We unambiguously resolve interlayer hole transfer (IHT) to WS_2 following selective excitation of the A exciton of MoS_2 with a 34 ± 14 fs time constant and furthermore resolve interlayer electron transfer (IET) to MoS_2 following excitation on resonance with the A exciton of WS_2 with a 69 ± 9 fs time constant. We corroborate our findings by comparing these results with 2DES measurements of the individual layered components of the HS.

Figure 1b reports a sketch of the band alignment at the K point for the WS_2/MoS_2 HS as calculated in ref 46. For clarity, we identify the A and B excitons of each layer of the HS with a subscript corresponding to the layer's transition metal (A_X and B_X where X = Mo or W). Single crystal millimeter-scale ML-TMDs are prepared via gold-tape exfoliation of bulk crystals.[45] The large-area WS_2/MoS_2 HS is obtained by vertically stacking the MLs and transferring them onto a transparent 200-μm-thick SiO_2 substrate;[45] an interlayer twist angle of 29.5 ± 0.9° was determined by polarization-resolved second harmonic generation measurements (Figure S3). The absorption spectrum of the HS at 80 K is shown in Figure 1c. The 2DES experiments are performed at 80 K using a partially collinear pump−probe geometry and measuring the real absorptive third-order nonlinear signal. The home-built 2DES instrument generates the pump−pulse pair with birefringent wedges, which scan the coherence time, t_1, with high phase stability.[47]

2DES maps plot the correlation between excitation energy ($\hbar\omega_1$) and detection energy ($\hbar\omega_3$) for a given waiting time, t_2. We begin by examining the 2DES maps of the real absorptive signal of the ML-MoS_2 (Figure 2a). The 2DES map at t_2 = 0

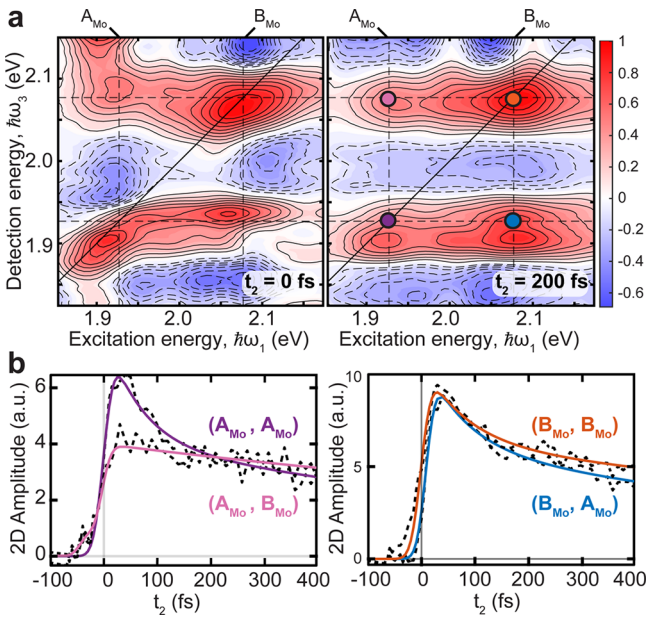

Figure 2. (a) 2DES maps of the real absorptive signal of ML-MoS_2 at 80 K at t_2 = 0 fs (left) and 200 fs (right). Positive (negative) sign signals are red (blue) with filled (dashed) contours drawn in 10% increments of the maximum. The incident pump fluence is 10 μJ/cm^2. Dashed lines indicate the energies of A_{Mo} (ω = 1.92 eV) and B_{Mo} (ω = 2.07 eV) excitons. (b) Values of t_2 dynamics of MoS_2 ML following excitation of the A_{Mo} (left) and B_{Mo} excitons (right). The t_2 traces are shown with fits color coded for dots in (a).

https://doi.org/10.1021/acs.nanolett.1c01098
Nano Lett. 2021, 21, 4738−4743

displays two positive diagonal ($\hbar\omega_1 = \hbar\omega_3$) peaks corresponding to photobleaching (PB) of A_{Mo} and B_{Mo} excitons. At early times, the diagonal peaks are inhomogeneously broadened along the diagonal due to the spatial heterogeneity of the sample, while the homogeneous line width lies along the antidiagonal direction. Spectral signatures of the off-diagonal or cross-peaks ($\hbar\omega_1 \neq \hbar\omega_3$) between A_{Mo} and B_{Mo} at $t_2 = 0$ fs indicate strong intralayer excitonic coupling, whereas the t_2-dependent behavior reports on intralayer exciton dynamics and coupling strengths. Strong coupling between the A and B excitons in ML-MoS_2[42,44,48] and other ML-TMDs[49] has been previously observed and ascribed to several mechanisms: light-induced band gap renormalization (BGR),[48] Dexter-like intervalley exciton coupling,[50] and intervalley exchange interaction,[42] among others.[49,51,52] At later times, all four peaks exhibit horizontal elongation along the excitation axis, consistent with previous observations, using ultrafast TA, of a delayed excitonic PB following above-resonance excitation.[53]

The early temporal dynamics of the ML-MoS_2 excitonic signatures are plotted as a function of waiting time, t_2, in Figure 2b. With the exception of the above-diagonal cross-peak at ($\hbar\omega_1$,$\hbar\omega_3$) = (A_{Mo},B_{Mo}) (pink circle), the signatures display an instantaneous rise and a double exponential decay within the 1 ps temporal window of the measurement. The ultrafast decay is consistent with previous observations and has been attributed to carrier thermalization and cooling.[54] The above-diagonal cross-peak is characterized by a slightly delayed PB formation followed by a single exponential decay. Similar dynamics of the (A_{Mo},B_{Mo}) peak were recently reported in a 2DES study of chemical vapor deposition grown ML-MoS_2 using a cocircularly polarized configuration and attributed to an excitonic exchange interaction.[42] Negative peaks in the 2D maps (blue, Figure 2a) are due to photoinduced absorption and are located at detection energies below the positive PB peaks. These features are attributed to many-body effects which are referred to cumulatively as BGR.[44,48]

The 2DES maps of the WS_2/MoS_2 HS (Figure 3a) show many distinct features compared to the ML-MoS_2. At $t_2 = 0$ fs, we see prominent diagonal peaks of the A_{Mo} and B_{Mo} PB, as in the ML-MoS_2 sample, with an additional diagonal peak from the A_W exciton. The A_W peak is red-shifted in comparison to the A_W of the ML-WS_2 (Figure S4) and is well separated spectrally from the A_{Mo} and B_{Mo} excitons. We attribute the spectral shift of A_W to differences in the dielectric environment of the WS_2 layer in the HS.[55,56] At $t_2 = 0$ fs, the WS_2/MoS_2 HS 2DES maps show significant broadening along the diagonal, due to overlap of the three inhomogeneously broadened excitons in close spectral proximity to one another. Similar to ML-MoS_2, Figure 3a shows signatures of strong intralayer coupling between the A_{Mo} and B_{Mo} excitons, resulting in cross-peaks present at $t_2 = 0$ fs. We are unable to resolve intralayer cross-peaks of the WS_2 layer as the B_W exciton falls outside our spectral detection window.

We can identify several spectral signatures unique to the HS which are the result of interlayer coupling and ICT processes. Several below-diagonal signatures of interlayer coupling are visible at $t_2 = 0$ fs at ($\hbar\omega_1$,$\hbar\omega_3$) = (B_{Mo},A_W) and (A_W,A_{Mo}). These signatures show an instantaneous rise similar to the diagonal peaks (Figure S7). At later times, additional interlayer cross-peaks grow in above the diagonal. The 2D map at t_2 = 200 fs shows a grid of positive PB signals between every possible combination of the three excitonic states along with weak negative BGR signals red-shifted along $\hbar\omega_3$ from each

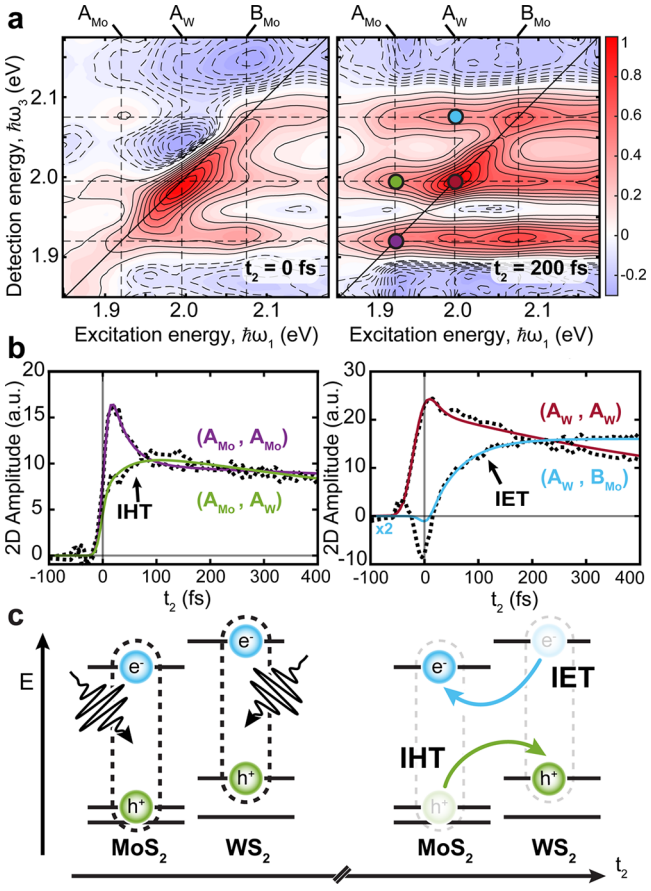

Figure 3. (a) 2DES maps of the real absorptive signal of WS_2/MoS_2 HS at 80 K for $t_2 = 0$ fs (left) and 200 fs (right). Dashed lines indicate the energies of A_{Mo} ($\hbar\omega$ = 1.92 eV), A_W ($\hbar\omega$ = 1.99 eV), and B_{Mo} ($\hbar\omega$ = 2.07 eV) excitons. The pump incident fluence is 13 μJ/cm^2. The photoinduced carrier density is estimated to be ~5.5 × 10^{12} cm^{-2} by considering the absorption coefficients of the individual layers. (b) Values of t_2 dynamics of ICT signatures. Signatures of IHT following excitation of the A_{Mo} exciton (left) show a delayed rising component at the detection energy of A_W. Signatures of IET following excitation of the A_W exciton (right) show a delayed rising component at the detection energy of B_{Mo}. The t_2 traces are shown with fits color coded for dots in (a). The (A_W,B_{Mo}) t_2 trace is multiplied by a factor of 2 for better comparison. (c) Cartoon illustrating the process of interlayer hole and electron transfer upon optical excitation of the MoS_2 and WS_2 layers, respectively.

excitonic resonance. The above-diagonal cross-peaks (green and cyan circles, Figure 3a) display a delayed PB signal. We assign these interlayer cross-peaks to ICT processes: IHT and IET for the peaks located at ($\hbar\omega_1$,$\hbar\omega_3$) = (A_{Mo},A_W) and (A_W,B_{Mo}), respectively.

The delayed PB at ($\hbar\omega_1$,$\hbar\omega_3$) = (A_{Mo},A_W) (Figure 3b) is consistent with a dissociation of A_{Mo} excitons, leading to ultrafast hole scattering from the upper VB of the MoS_2 to the higher-energy upper VB in the WS_2 at the K(K′) point (Figure 3c). To confirm this assignment, we compare to the 2DES data of ML-MoS_2 and ML-WS_2. The t_2 dynamics of the ML-MoS_2 sample taken at the same excitation/detection energy as the IHT signature shows a completely different behavior: an instantaneous buildup and a negative signal due to the BGR upon A_{Mo} resonant photoexcitation (Figure S8). The isolated ML-WS_2 sample (Figure S4) gives rise to a negligible signal because the excitation energy is below the optical gap of the

https://doi.org/10.1021/acs.nanolett.1c01098
Nano Lett. 2021, 21, 4738−4743

material. We can then attribute the delayed rise of the cross-peak in the HS to IHT.

The above diagonal t_2 dynamics of the peak at $(\hbar\omega_1,\hbar\omega_3) = (A_W,B_{Mo})$ (Figure 3b) shows a slightly slower buildup of the PB signature following excitation of the A_W exciton, which is consistent with the dissociation of the A_W exciton due to the scattering of the electron from the CB of WS_2 to the lower energy CB of MoS_2 at the K(K′) points. In this case, however, the excitation resonant with the A_W exciton photoinjects electron/hole pairs into both the TMD layers, and so we expect that the PB of the cross-peak would have an additional contribution given by the combination of Pauli blocking and many-body correlation effects due to electron/hole pairs directly photoexcited above the optical gap of MoS_2. Again, the t_2 dynamics of the isolated MoS_2 and WS_2 layers, measured at the same excitation/emission energy as the IET signature, do not display any retarded buildup time, as reported in Figure S9. This comparison clearly shows that the t_2 dynamics of the HS is not a mere sum of the dynamics of the two TMD layers, and therefore, the slow rise time of the (A_W,B_{Mo}) peak can be mostly attributed to the IET process.

To quantify the time scales of the delayed PB signatures of ICT processes, we fit the buildup t_2 dynamics with the convolution between a rising exponential and a Gaussian instrument response function accounting for the finite temporal resolution of the experiment (a sum of decaying exponentials is used to fit the relaxation dynamics). More details of the fitting model and the fitting results can be found in the Supporting Information. The interlayer cross-peak at $(\hbar\omega_1,\hbar\omega_3) = (A_{Mo},A_W)$ is fit with a 34 ± 14 fs fast growth component and 1.2 ± 0.1 ps decay component, which is the result of intra- and interlayer recombination processes (Figure S7). A sub-100 fs time scale was tentatively claimed for hole transfer process by previous TA measurements on the same HS, but the lack of high temporal resolution hindered the precise characterization of the scattering process.[19,23,25] The IET dynamics at $(\hbar\omega_1,\hbar\omega_3) = (A_W,B_{Mo})$ displays a slightly slower rise time that has been fitted to be 69 ± 9 fs (Figure S7). Recent time-resolved angle-resolved photoemission spectroscopy measurements[26] are consistent with this time scale and show that photoexcited electrons in the K valley can spread their occupation on a broad momentum space, quickly scattering to other valleys which display strong layer hybridization. Sub-100 fs intervalley scattering of electrons in the CB and strong valley hybridization could then facilitate IET process. Slower IET time with respect to IHT was predicted, although overestimated, by theoretical calculations and attributed to the weaker donor−acceptor coupling and shorter quantum coherence.[57] We emphasize that the accurate measurement of the ICT times in this study is only possible due to the combination of high temporal and spectral resolution of the 2DES technique. The fitting also reveals additional differences between the ML-MoS_2 and the HS. We find that the above-diagonal intralayer cross-peak (A_{Mo},B_{Mo}) in the HS shows a formation time (i.e., 90 ± 20 fs) more delayed than that in the ML-MoS_2 (<20 fs) (see Figure S5). This effect can be explained as a result of a competition between the exchange coupling between A/B excitons of ML-MoS_2 and the IHT process. The depletion of the A exciton population might result in a decreased interaction with the higher energy B exciton and, as a consequence, further increase of the (A_{Mo},B_{Mo}) cross-peak formation time scale.

We have focused on the two above-diagonal signatures of ICT for our analysis thus far, though two additional signatures of ICT are expected below the diagonal in Figure 3a. As described above, the below-diagonal (A_W,A_{Mo}) and (B_{Mo},A_W) peaks are characterized by pulse-width-limited buildup dynamics with overlapping signals which are determined by both intralayer and interlayer scattering processes. The absence of delayed formation in the PB peaks of the below diagonal cross-peaks is a signature that the former of these processes prevails and determines the formation dynamics. This result is supported by recent experiments showing that electron−hole pairs photoexcited above the optical gap of TMDs relax on the bottom (top) of the CB (VB) at the K point on time scale faster than 20 fs.[53]

In conclusion, we have performed broadband 2DES on a large-area WS_2/MoS_2 HS, covering simultaneously the A and B excitons of MoS_2 and the A exciton of WS_2. We unambiguously observe IHT to WS_2 with 34 ± 14 fs time constant following excitation of the A_{Mo} exciton and IET to MoS_2 with 69 ± 9 fs time constant following excitation of the A_W exciton. Our results demonstrate the ability of 2DES, due to its unique combination of high temporal and spectral resolution, to distinguish between various excitonic dynamics in a spectrally congested TMD-HSs, overcoming the limitations of conventional TA spectroscopy. Continuing to implement 2DES on different large-area TMD-HS samples will allow us to characterize the extremely rapid exciton and charge carrier dynamics and their dependence on interlayer tilt angle, among many other variables.

■ ASSOCIATED CONTENT

Supporting Information

The Supporting Information is available free of charge at https://pubs.acs.org/doi/10.1021/acs.nanolett.1c01098.

Two-dimensional electronic spectroscopy (2DES); 2DES setup; pulse characterization; large-area sample preparation and characterization of interlayer twist angle; 2DES map of isolated WS_2; fitting procedure and time constants; supplementary data (PDF)

■ AUTHOR INFORMATION

Corresponding Authors

Xiaoyang Zhu − *Department of Chemistry, Columbia University, New York 10027, United States;* orcid.org/0000-0002-2090-8484; Email: xyzhu@columbia.edu

Stefano Dal Conte − *IFN-CNR, Dipartimento di Fisica, Politecnico di Milano, 20133 Milano, Italy;* orcid.org/0000-0001-8582-3185; Email: stefano.dalconte@polimi.it

Giulio Cerullo − *IFN-CNR, Dipartimento di Fisica, Politecnico di Milano, 20133 Milano, Italy;* orcid.org/0000-0002-9534-2702; Email: giulio.cerullo@polimi.it

Authors

Veronica R. Policht − *IFN-CNR, Dipartimento di Fisica, Politecnico di Milano, 20133 Milano, Italy;* orcid.org/0000-0002-1781-7258

Mattia Russo − *IFN-CNR, Dipartimento di Fisica, Politecnico di Milano, 20133 Milano, Italy*

Fang Liu − *Department of Chemistry, Stanford University, Stanford, California 94305, United States*

https://doi.org/10.1021/acs.nanolett.1c01098
Nano Lett. 2021, 21, 4738−4743

Chiara Trovatello − *IFN-CNR, Dipartimento di Fisica, Politecnico di Milano, 20133 Milano, Italy;* orcid.org/0000-0002-8150-9743

Margherita Maiuri − *IFN-CNR, Dipartimento di Fisica, Politecnico di Milano, 20133 Milano, Italy;* orcid.org/0000-0001-9351-8551

Yusong Bai − *Department of Chemistry, Columbia University, New York 10027, United States*

Complete contact information is available at: https://pubs.acs.org/10.1021/acs.nanolett.1c01098

Author Contributions

X.Y.Z., S.D.C., and G.C. conceived the research. F.L. prepared the TMD-HS samples. V.R.P. and M.R. performed the 2DES experiments. V.R.P., M.R., C.T., M.M., and S.D.C. analyzed and interpreted the experimental data. Y.B. performed the SHG experiment. The paper was written by V.R.P. and S.D.C. with input from all authors. X.Y.Z. and G.C. supervised and coordinated the project.

Notes

The authors declare no competing financial interest.

■ ACKNOWLEDGMENTS

G.C. acknowledges the support by the European Union Horizon 2020 Programme under Grant Agreement No. 881603 Graphene Core 3 and by the PRIN 2017 Project 201795SBA3−HARVEST. S.D.C. and C.T. acknowledge funding from PRIN 2017 Programme (Prot. 20172H2SC4) from the MIUR. X.Y.Z. acknowledges support by the Materials Science and Engineering Research Center (MRSEC) through NSF Grant No. DMR-2011738.

■ REFERENCES

(1) Mak, K. F.; Lee, C.; Hone, J.; Shan, J.; Heinz, T. F. Atomically Thin MoS2: A New Direct-Gap Semiconductor. *Phys. Rev. Lett.* **2010**, *105* (13), 136805.

(2) Wang, Q. H.; Kalantar-Zadeh, K.; Kis, A.; Coleman, J. N.; Strano, M. S. Electronics and Optoelectronics of Two-Dimensional Transition Metal Dichalcogenides. *Nat. Nanotechnol.* **2012**, *7* (11), 699−712.

(3) Wang, G.; Chernikov, A.; Glazov, M. M.; Heinz, T. F.; Marie, X.; Amand, T.; Urbaszek, B. Colloquium : Excitons in Atomically Thin Transition Metal Dichalcogenides. *Rev. Mod. Phys.* **2018**, *90* (2), 021001.

(4) Schaibley, J. R.; Yu, H.; Clark, G.; Rivera, P.; Ross, J. S.; Seyler, K. L.; Yao, W.; Xu, X. Valleytronics in 2D Materials. *Nat. Rev. Mater.* **2016**, *1* (11), 16055.

(5) Mueller, T.; Malic, E. Exciton Physics and Device Application of Two-Dimensional Transition Metal Dichalcogenide Semiconductors. *npj 2D Mater. Appl.* **2018**, *2* (1), 29.

(6) Liu, Y.; Weiss, N. O.; Duan, X.; Cheng, H.-C.; Huang, Y.; Duan, X. Van Der Waals Heterostructures and Devices. *Nat. Rev. Mater.* **2016**, *1* (9), 16042.

(7) Zhang, W.; Wang, Q.; Chen, Y.; Wang, Z.; Wee, A. T. S. Van Der Waals Stacked 2D Layered Materials for Optoelectronics. *2D Mater.* **2016**, *3* (2), 022001.

(8) Rivera, P.; Schaibley, J. R.; Jones, A. M.; Ross, J. S.; Wu, S.; Aivazian, G.; Klement, P.; Seyler, K.; Clark, G.; Ghimire, N. J.; Yan, J.; Mandrus, D. G.; Yao, W.; Xu, X. Observation of Long-Lived Interlayer Excitons in Monolayer MoSe2−WSe2 Heterostructures. *Nat. Commun.* **2015**, *6* (1), 6242.

(9) Nagler, P.; Plechinger, G.; Ballottin, M. V.; Mitioglu, A.; Meier, S.; Paradiso, N.; Strunk, C.; Chernikov, A.; Christianen, P. C. M.; Schüller, C.; Korn, T. Interlayer Exciton Dynamics in a Dichalcogenide Monolayer Heterostructure. *2D Mater.* **2017**, *4* (2), 025112.

(10) Miller, B.; Steinhoff, A.; Pano, B.; Klein, J.; Jahnke, F.; Holleitner, A.; Wurstbauer, U. Long-Lived Direct and Indirect Interlayer Excitons in van Der Waals Heterostructures. *Nano Lett.* **2017**, *17* (9), 5229−5237.

(11) Robert, C.; Lagarde, D.; Cadiz, F.; Wang, G.; Lassagne, B.; Amand, T.; Balocchi, A.; Renucci, P.; Tongay, S.; Urbaszek, B.; Marie, X. Exciton Radiative Lifetime in Transition Metal Dichalcogenide Monolayers. *Phys. Rev. B: Condens. Matter Mater. Phys.* **2016**, *93* (20), 205423.

(12) Unuchek, D.; Ciarrocchi, A.; Avsar, A.; Watanabe, K.; Taniguchi, T.; Kis, A. Room-Temperature Electrical Control of Exciton Flux in a van Der Waals Heterostructure. *Nature* **2018**, *560* (7718), 340−344.

(13) Yuan, L.; Zheng, B.; Kunstmann, J.; Brumme, T.; Kuc, A. B.; Ma, C.; Deng, S.; Blach, D.; Pan, A.; Huang, L. Twist-Angle-Dependent Interlayer Exciton Diffusion in WS2−WSe2 Heterobilayers. *Nat. Mater.* **2020**, *19* (6), 617−623.

(14) Jin, C.; Kim, J.; Utama, M. I. B.; Regan, E. C.; Kleemann, H.; Cai, H.; Shen, Y.; Shinner, M. J.; Sengupta, A.; Watanabe, K.; Taniguchi, T.; Tongay, S.; Zettl, A.; Wang, F. Imaging of Pure Spin-Valley Diffusion Current in WS2-WSe2 Heterostructures. *Science (Washington, DC, U. S.)* **2018**, *360* (6391), 893−896.

(15) Unuchek, D.; Ciarrocchi, A.; Avsar, A.; Sun, Z.; Watanabe, K.; Taniguchi, T.; Kis, A. Valley-Polarized Exciton Currents in a van Der Waals Heterostructure. *Nat. Nanotechnol.* **2019**, *14* (12), 1104−1109.

(16) Ajayan, P.; Kim, P.; Banerjee, K. Two-Dimensional van Der Waals Materials. *Phys. Today* **2016**, *69* (9), 38−44.

(17) Ceballos, F.; Zhao, H. Ultrafast Laser Spectroscopy of Two-Dimensional Materials Beyond Graphene. *Adv. Funct. Mater.* **2017**, *27* (19), 1604509.

(18) Dal Conte, S.; Trovatello, C.; Gadermaier, C.; Cerullo, G. Ultrafast Photophysics of 2D Semiconductors and Related Heterostructures. *Trends Chem.* **2020**, *2* (1), 28−42.

(19) Hong, X.; Kim, J.; Shi, S. F.; Zhang, Y. Y.; Jin, C.; Sun, Y.; Tongay, S.; Wu, J.; Zhang, Y. Y.; Wang, F. Ultrafast Charge Transfer in Atomically Thin MoS2/WS2 Heterostructures. *Nat. Nanotechnol.* **2014**, *9* (9), 682−686.

(20) Ceballos, F.; Bellus, M. Z.; Chiu, H.-Y.; Zhao, H. Ultrafast Charge Separation and Indirect Exciton Formation in a MoS2−MoSe2 van Der Waals Heterostructure. *ACS Nano* **2014**, *8* (12), 12717−12724.

(21) Zhu, H.; Wang, J.; Gong, Z.; Kim, Y. D.; Hone, J.; Zhu, X.-Y. Interfacial Charge Transfer Circumventing Momentum Mismatch at Two-Dimensional van Der Waals Heterojunctions. *Nano Lett.* **2017**, *17* (6), 3591−3598.

(22) Rigosi, A. F.; Hill, H. M.; Li, Y.; Chernikov, A.; Heinz, T. F. Probing Interlayer Interactions in Transition Metal Dichalcogenide Heterostructures by Optical Spectroscopy: MoS2/WS2 and MoSe2/WSe2. *Nano Lett.* **2015**, *15* (8), 5033−5038.

(23) Chen, H.; Wen, X.; Zhang, J.; Wu, T.; Gong, Y.; Zhang, X.; Yuan, J.; Yi, C.; Lou, J.; Ajayan, P. M.; Zhuang, W.; Zhang, G.; Zheng, J. Ultrafast Formation of Interlayer Hot Excitons in Atomically Thin MoS2/WS2 Heterostructures. *Nat. Commun.* **2016**, *7* (1), 12512.

(24) Wang, K.; Huang, B.; Tian, M.; Ceballos, F.; Lin, M.-W.; Mahjouri-Samani, M.; Boulesbaa, A.; Puretzky, A. A.; Rouleau, C. M.; Yoon, M.; Zhao, H.; Xiao, K.; Duscher, G.; Geohegan, D. B. Interlayer Coupling in Twisted WSe2/WS2 Bilayer Heterostructures Revealed by Optical Spectroscopy. *ACS Nano* **2016**, *10* (7), 6612−6622.

(25) Ji, Z.; Hong, H.; Zhang, J.; Zhang, Q.; Huang, W.; Cao, T.; Qiao, R.; Liu, C.; Liang, J.; Jin, C.; Jiao, L.; Shi, K.; Meng, S.; Liu, K. Robust Stacking-Independent Ultrafast Charge Transfer in MoS2/WS2 Bilayers. *ACS Nano* **2017**, *11* (12), 12020−12026.

(26) Liu, F.; Li, Q.; Zhu, X. Y. Direct Determination of Momentum-Resolved Electron Transfer in the Photoexcited van Der Waals Heterobilayer WS2/MoS2. *Phys. Rev. B: Condens. Matter Mater. Phys.* **2020**, *101* (20), 201405.

(27) Heo, H.; Sung, J. H.; Cha, S.; Jang, B.-G.; Kim, J.-Y.; Jin, G.; Lee, D.; Ahn, J.-H.; Lee, M.-J.; Shim, J. H.; Choi, H.; Jo, M.-H. Interlayer Orientation-Dependent Light Absorption and Emission in Monolayer Semiconductor Stacks. *Nat. Commun.* **2015**, *6* (1), 7372.
(28) Liu, J.; Zhang, X.; Lu, G. Excitonic Effect Drives Ultrafast Dynamics in van Der Waals Heterostructures. *Nano Lett.* **2020**, *20* (6), 4631−4637.
(29) Wang, Y.; Wang, Z.; Yao, W.; Liu, G.-B.; Yu, H. Interlayer Coupling in Commensurate and Incommensurate Bilayer Structures of Transition-Metal Dichalcogenides. *Phys. Rev. B: Condens. Matter Mater. Phys.* **2017**, *95* (11), 115426.
(30) Okada, M.; Kutana, A.; Kureishi, Y.; Kobayashi, Y.; Saito, Y.; Saito, T.; Watanabe, K.; Taniguchi, T.; Gupta, S.; Miyata, Y.; Yakobson, B. I.; Shinohara, H.; Kitaura, R. Direct and Indirect Interlayer Excitons in a van Der Waals Heterostructure of HBN/WS2/MoS2/HBN. *ACS Nano* **2018**, *12* (3), 2498−2505.
(31) Wilson, N. R.; Nguyen, P. V.; Seyler, K.; Rivera, P.; Marsden, A. J.; Laker, Z. P. L.; Constantinescu, G. C.; Kandyba, V.; Barinov, A.; Hine, N. D. M.; Xu, X.; Cobden, D. H. Determination of Band Offsets, Hybridization, and Exciton Binding in 2D Semiconductor Heterostructures. *Sci. Adv.* **2017**, *3* (2), No. e1601832.
(32) Torun, E.; Miranda, H. P. C.; Molina-Sánchez, A.; Wirtz, L. Interlayer and Intralayer Excitons in MoS2/WS2 and MoSe2/WSe2 Heterobilayers. *Phys. Rev. B: Condens. Matter Mater. Phys.* **2018**, *97* (24), 245427.
(33) Long, R.; Prezhdo, O. V. Quantum Coherence Facilitates Efficient Charge Separation at a MoS2/MoSe2 van Der Waals Junction. *Nano Lett.* **2016**, *16* (3), 1996−2003.
(34) Brixner, T.; Mančal, T.; Stiopkin, I. V.; Fleming, G. R. Phase-Stabilized Two-Dimensional Electronic Spectroscopy. *J. Chem. Phys.* **2004**, *121* (9), 4221−4236.
(35) Hybl, J. D.; Albrecht Ferro, A.; Jonas, D. M. Two-Dimensional Fourier Transform Electronic Spectroscopy. *J. Chem. Phys.* **2001**, *115* (14), 6606.
(36) Fuller, F. D.; Ogilvie, J. P. Experimental Implementations of Two-Dimensional Fourier Transform Electronic Spectroscopy. *Annu. Rev. Phys. Chem.* **2015**, *66* (1), 667−690.
(37) Ogilvie, J. P.; Kubarych, K. J. Multidimensional Electronic and Vibrational Spectroscopy. In *Advances in Atomic, Molecular and Optical Physics*; Elsevier, 2009; Vol. *57*, pp 249−321.
(38) Hao, K.; Specht, J. F.; Nagler, P.; Xu, L.; Tran, K.; Singh, A.; Dass, C. K.; Schüller, C.; Korn, T.; Richter, M.; Knorr, A.; Li, X.; Moody, G. Neutral and Charged Inter-Valley Biexcitons in Monolayer MoSe2. *Nat. Commun.* **2017**, *8*, 15552.
(39) Hao, K.; Moody, G.; Wu, F.; Dass, C. K.; Xu, L.; Chen, C.; Sun, L.; Li, M.-Y.; Li, L.; Macdonald, A. H.; Li, X. Direct Measurement of Exciton Valley Coherence in Monolayer WSe2. *Nat. Phys.* **2016**, *12* (7), 677−682.
(40) Martin, E. W.; Horng, J.; Hanna, G. R.; Paik, E.; Wentzel, M.-H.; Deng, H.; Steven, T. C. Encapsulation Narrows Excitonic Homogeneous Linewidth of Exfoliated MoSe2Monolayer. *EPJ Web Conf.* **2019**, *205*, 06021.
(41) Ruth, H. G.; Martin, E. W.; Purz, T. L.; Rivera, P.; Xu, X.; Cundiff, S. T. Direct Measurement of Coherent Coupling in a $MoSe_2/WSe_2$ Heterostructure. In *Conference on Lasers and Electro-Optics*; Cerullo, G., Ogilvie, J., Kärtner, F., Khalil, M., Li, R., Eds.; OSA: Washington, D.C., 2019; p FW3M.2.
(42) Guo, L.; Wu, M.; Cao, T.; Monahan, D. M.; Lee, Y. H.; Louie, S. G.; Fleming, G. R. Exchange-Driven Intravalley Mixing of Excitons in Monolayer Transition Metal Dichalcogenides. *Nat. Phys.* **2019**, *15* (3), 228−232.
(43) Maiuri, M.; Conte, S. D.; Russo, M.; Wang, J.; Soavi, G.; Dumcenco, D.; Kis, A.; Selig, M.; Khun, S.; Richter, M.; Knorr, A.; Ferrari, A. C.; Cerullo, G. Excitonic Effects in Single Layer MoS_2 Probed by Broadband Two-Dimensional Electronic Spectroscopy. *Conference on Lasers and Electro-Optics*; OSA: Washington, D.C., 2019; Vol. *37*, p FW3M.4.
(44) Wood, R. E.; Lloyd, L. T.; Mujid, F.; Wang, L.; Allodi, M. A.; Gao, H.; Mazuski, R.; Ting, P.; Xie, S.; Park, J.; Engel, G. S. Evidence for the Dominance of Carrier-Induced Band Gap Renormalization over Biexciton Formation in Cryogenic Ultrafast Experiments on MoS2Monolayers. *J. Phys. Chem. Lett.* **2020**, *11*, 2658−2666.
(45) Liu, F.; Wu, W.; Bai, Y.; Chae, S. H.; Li, Q.; Wang, J.; Hone, J.; Zhu, X.-Y. Disassembling 2D van Der Waals Crystals into Macroscopic Monolayers and Reassembling into Artificial Lattices. *Science (Washington, DC, U. S.)* **2020**, *367* (6480), 903−906.
(46) Komsa, H. P.; Krasheninnikov, A. V. Electronic Structures and Optical Properties of Realistic Transition Metal Dichalcogenide Heterostructures from First Principles. *Phys. Rev. B: Condens. Matter Mater. Phys.* **2013**, *88* (8), 085318.
(47) Réhault, J.; Maiuri, M.; Oriana, A.; Cerullo, G. Two-Dimensional Electronic Spectroscopy with Birefringent Wedges. *Rev. Sci. Instrum.* **2014**, *85* (12), 123107.
(48) Pogna, E. A. A.; Marsili, M.; De Fazio, D.; Dal Conte, S.; Manzoni, C.; Sangalli, D.; Yoon, D.; Lombardo, A.; Ferrari, A. C.; Marini, A.; Cerullo, G.; Prezzi, D. Photo-Induced Bandgap Renormalization Governs the Ultrafast Response of Single-Layer MoS2. *ACS Nano* **2016**, *10* (1), 1182−1188.
(49) Wang, Z.; Molina-Sánchez, A.; Altmann, P.; Sangalli, D.; De Fazio, D.; Soavi, G.; Sassi, U.; Bottegoni, F.; Ciccacci, F.; Finazzi, M.; Wirtz, L.; Ferrari, A. C.; Marini, A.; Cerullo, G.; Dal Conte, S. Intravalley Spin−Flip Relaxation Dynamics in Single-Layer WS2. *Nano Lett.* **2018**, *18* (11), 6882−6891.
(50) Berghäuser, G.; Bernal-Villamil, I.; Schmidt, R.; Schneider, R.; Niehues, I.; Erhart, P.; Michaelis De Vasconcellos, S.; Bratschitsch, R.; Knorr, A.; Malic, E. Inverted Valley Polarization in Optically Excited Transition Metal Dichalcogenides. *Nat. Commun.* **2018**, *9* (1), 971.
(51) Selig, M.; Katsch, F.; Schmidt, R.; Michaelis de Vasconcellos, S.; Bratschitsch, R.; Malic, E.; Knorr, A. Ultrafast Dynamics in Monolayer Transition Metal Dichalcogenides: Interplay of Dark Excitons, Phonons, and Intervalley Exchange. *Phys. Rev. Res.* **2019**, *1* (2), 022007.
(52) Manca, M.; Glazov, M. M.; Robert, C.; Cadiz, F.; Taniguchi, T.; Watanabe, K.; Courtade, E.; Amand, T.; Renucci, P.; Marie, X.; Wang, G.; Urbaszek, B. Enabling Valley Selective Exciton Scattering in Monolayer WSe2 through Upconversion. *Nat. Commun.* **2017**, *8*, 14927.
(53) Trovatello, C.; Katsch, F.; Borys, N. J.; Selig, M.; Yao, K.; Borrego-Varillas, R.; Scotognella, F.; Kriegel, I.; Yan, A.; Zettl, A.; Schuck, P. J.; Knorr, A.; Cerullo, G.; Conte, S. D. The Ultrafast Onset of Exciton Formation in 2D Semiconductors. *Nat. Commun.* **2020**, *11* (1), 5277.
(54) Nie, Z.; Long, R.; Sun, L.; Huang, C. C.; Zhang, J.; Xiong, Q.; Hewak, D. W.; Shen, Z.; Prezhdo, O. V.; Loh, Z. H. Ultrafast Carrier Thermalization and Cooling Dynamics in Few-Layer MoS2. *ACS Nano* **2014**, *8* (10), 10931−10940.
(55) Raja, A.; Chaves, A.; Yu, J.; Arefe, G.; Hill, H. M.; Rigosi, A. F.; Berkelbach, T. C.; Nagler, P.; Schüller, C.; Korn, T.; Nuckolls, C.; Hone, J.; Brus, L. E.; Heinz, T. F.; Reichman, D. R.; Chernikov, A. Coulomb Engineering of the Bandgap and Excitons in Two-Dimensional Materials. *Nat. Commun.* **2017**, *8* (May), 15251.
(56) Raja, A.; Waldecker, L.; Zipfel, J.; Cho, Y.; Brem, S.; Ziegler, J. D.; Kulig, M.; Taniguchi, T.; Watanabe, K.; Malic, E.; Heinz, T. F.; Berkelbach, T. C.; Chernikov, A. Dielectric Disorder in Two-Dimensional Materials. *Nat. Nanotechnol.* **2019**, *14* (9), 832−837.
(57) Li, L.; Long, R.; Prezhdo, O. V. Charge Separation and Recombination in Two-Dimensional MoS2/WS2 : Time-Domain Ab Initio Modeling. *Chem. Mater.* **2017**, *29* (6), 2466−2473.

https://doi.org/10.1021/acs.nanolett.1c01098
Nano Lett. 2021, 21, 4738−4743